Piezoelectric energy harvesting for civil infrastructure system applications: Moving loads and surface strain fluctuations

Alper Erturk

Abstract

This article formulates the problem of vibration-based energy harvesting using piezoelectric transduction for civil infrastructure system applications with a focus on moving load excitations and surface strain fluctuations. Two approaches of piezoelectric power generation from moving loads are formulated. The first one is based on using a bimorph cantilever located at an arbitrary position on a simply supported slender bridge. The fundamental moving load problem is reviewed and the input to the cantilevered energy harvester is obtained to couple with the generalized electromechanical equations for transient excitation. The second approach considers using a thin piezoceramic patch covering a region on the bridge. The transient electrical response of the surface patch to moving load excitation is derived in the presence of a resistive electrical load. The local way of formulating piezoelectric energy harvesting from two-dimensional surface strain fluctuations of large structures is also discussed. For a thin piezoceramic patch attached onto the surface of a large structure, analytical expressions of the electrical power output are presented for generalized, harmonic, and white noise–type two-dimensional strain fluctuations. Finally, a case study is given to analyze a small piezoceramic patch for energy harvesting from surface strain fluctuations along with measured bridge strain data.

Introduction

Vibration-based energy harvesting has received growing attention over the last decade (Anton and Sodano, 2007; Beeby et al., 2006; Cook-Chennault et al., 2008; Sodano et al., 2004). The basic motivation in this research field is due to the reduced power requirement of small electronic components, such as the wireless sensor networks used in passive and active monitoring applications. If such wireless electronic components can be powered by the vibrational energy available in their environment, the maintenance costs for periodic battery replacement as well as the resulting chemical waste of conventional batteries can be reduced dramatically.

The basic transduction mechanisms used for vibration-to-electric energy conversion are the electromagnetic (Mann and Sims, 2009), electrostatic (Chiu and Tseng, 2008), and piezoelectric (Erturk and Inman, 2009) transduction mechanisms. There have been recent articles focusing on the use of magnetostriction (Wang and Yuan, 2008) and electroactive polymers (Aureli et al., 2010) as well. Among these alternative

techniques for converting ambient vibrations into electricity, piezoelectric transduction has been studied most heavily (Anton and Sodano, 2007; Cook-Chennault et al., 2008; Sodano et al., 2004) primarily due to the ease of application and large power density of piezoelectric materials (Cook-Chennault et al., 2008). In the last few years, researchers have investigated various problems related to modeling (Elvin and Elvin, 2009; Erturk and Inman, 2009; Renno et al., 2009; Shu et al., 2007; Stanton et al., 2010a, b) and applications (Anton and Sodano, 2007; Cook-Chennault et al., 2008; Sodano et al., 2004) of piezoelectric energy harvesters.

Recent research in the field of vibration-based energy harvesting has focused on modeling and exploiting nonlinear dynamics (Cottone et al., 2009; Erturk

Georgia Institute of Technology, G. W. Woodruff School of Mechanical Engineering, Atlanta, GA 30332-0405, USA

Corresponding author:
Alper Erturk, Georgia Institute of Technology, 771 Ferst Drive, Love Building, Room 126, Atlanta, GA 30332-0405, USA
Email: alper.erturk@me.gatech.edu

et al., 2009a; Erturk and Inman, 2011a; Mann and Sims, 2009; Stanton et al., 2009, 2010a, b) as well as stochastic excitation (Adhikari et al., 2009; Daqaq, 2010; Halvorsen, 2008; Litak et al., 2010; Scruggs, 2009) of vibration-based energy harvesters. Although civil infrastructure systems constitute a unique application field for energy harvesting due to the common use of battery-powered wireless sensors (Elvin et al., 2003, 2006), such as the acoustic emission sensors (Ozevin et al., 2006; Shigeishi et al., 2001) used for structural health prognosis in bridges, electromechanical modeling of the fundamental civil engineering problems for vibration-based energy harvesting has not been discussed in the literature. The aim of this article is to provide an introduction to formulating such problems by focusing on piezoelectric energy harvesting for typical civil infrastructure system applications. The problems considered in this article are the moving load excitation of slender bridges and the surface strain fluctuations of large structures for piezoelectric power generation.

In the following sections, first a cantilevered piezoelectric energy harvester model is summarized for harmonic, arbitrary transient, and white noise excitations. After that, the fundamental moving load problem is visited for piezoelectric energy harvesting by considering two scenarios. In the first scenario, a cantilevered energy harvester is located at an arbitrary point on the bridge and a systematic approach is discussed for relating the moving load problem to the distributed parameter electromechanical equations of the energy harvester. In the second scenario, a piezoceramic patch covers a region on the bridge and analytical derivations are given to relate the piezoelectric power output delivered from the patch to a resistive electrical load in terms of the moving load excitation. After the fundamental moving load problem, the focus is placed on formulating the piezoelectric energy-harvesting problem from two-dimensional surface strain fluctuations on large structures. Considering the orthogonal strain fluctuations as the excitation input to a rectangular piezoceramic patch, analytical expressions for the electrical power output are obtained for generalized, harmonic, and white noise inputs. Finally, a case study is given to analyze a small piezoceramic patch for power generation from surface strain fluctuations. The power generation potential of a small piezoelectric patch is discussed based on the strain measurements for a steel multigirder bridge.

Piezoelectric Energy Harvesting from Base Excitation of Bimorph Cantilevers

This section summarizes the analytical derivations for a bimorph cantilever located on and excited by vibrations of a host civil engineering structure. The governing electromechanical equations are given for a generalized base acceleration input, which are then solved for the steady-state electromechanical response for harmonic base acceleration. Following the harmonic excitation case, the governing equations are expressed in the first-order form for transient base acceleration inputs (which is the typical case in the moving load problem). Response to broadband random base vibration is also covered at the end of this section.

Governing Electromechanical Equations

The cantilevered energy harvester configurations shown in Figure 1 are geometrically uniform symmetric thin bimorphs (made of two identical piezoceramic layers bracketing an elastic substructure layer) and they are excited under base vibration. The original model (Erturk and Inman, 2009) assumes the base motion to be translation in the transverse direction with superimposed small rotation while the derivation given here ignores the base rotation. A tip mass (proof mass) is attached rigidly at the free end to tune the natural frequencies (usually the focus is placed on the fundamental natural frequency). The perfectly conductive electrodes of negligible thickness fully cover the transverse faces of the piezoceramic layers, and the wiring cases shown in Figures 1(a) and (b) represent the series and parallel connections of the electrical outputs (to the external resistive load), respectively. The problem of interest in vibration-based energy harvesting is to express the power delivered to the electrical load in terms of the base acceleration input.

The linear electroelastic dynamics of a thin bimorph piezoelectric energy harvester beam under base excitation are governed by the following equations (Erturk and Inman, 2009):

$$D\frac{\partial^4 w_{rel}(x,t)}{\partial x^4} + c_s \frac{\partial^5 w_{rel}(x,t)}{\partial x^4 \partial t} + c_m \frac{\partial w_{rel}(x,t)}{\partial t} + m\frac{\partial^2 w_{rel}(x,t)}{\partial t^2}$$
$$-\vartheta v(t)\left[\frac{\mathrm{d}\delta(x)}{\mathrm{d}x} - \frac{\mathrm{d}\delta(x-L)}{\mathrm{d}x}\right] = -[m + M_t \delta(x-L)]a(t)$$
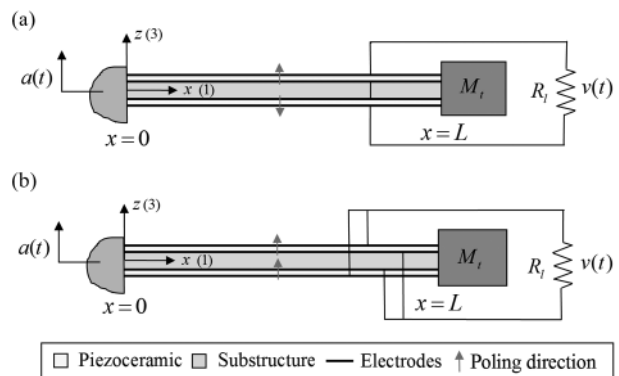
$$(1)$$

Figure 1. Cantilevered bimorph piezoelectric energy harvester configurations under base excitation: (a) series connection and (b) parallel connection.

$$C_p^{eq}\frac{\mathrm{d}v(t)}{\mathrm{d}t} + \frac{v(t)}{R_l} + \vartheta\int_0^L \frac{\partial^3 w_{rel}(x,t)}{\partial x^2 \partial t}\,\mathrm{d}x = 0 \qquad (2)$$

where $a(t)$ is the translational base acceleration in the transverse direction, $w_{rel}(x,t)$ is the vibration response (transverse displacement of the neutral axis relative to the moving base at position x and time t), $v(t)$ is the voltage response (across the external resistive load R_l), D is the bending stiffness of the beam, m is the mass per unit length of the beam, c_m is the external (air) damping coefficient (mass proportional damping), c_s is the internal (strain rate or Kelvin–Voigt) damping coefficient of the composite structure (stiffness proportional damping), M_t is the tip mass, C_p^{eq} is the equivalent capacitance of the piezoceramic layers, ϑ is the electromechanical coupling term in the physical coordinates, and $\delta(x)$ is the Dirac delta function. The electromechanical coupling term is $\vartheta = \bar{e}_{31}bh_{pc}$ if the layers are connected in series, whereas it is $\vartheta = 2\bar{e}_{31}bh_{pc}$ if the layers are connected in parallel (where $\bar{e}_{31}$ is the plane-stress piezoelectric stress constant, b is the width of the layers, and h_{pc} is the distance from the neutral axis to the center of each piezoceramic layer: $h_{pc} = (h_p + h_s)/2$, where h_p is the thickness of each piezoceramic layer and h_s is the thickness of the substructure layer).

Based on the standard modal analysis procedure (Meirovitch, 2001), that is, assuming the system to be a normal-mode system,[1] the vibration response is expressed in terms of the modal coordinates $\eta_r(t)$ and the mode shapes (mass-normalized eigenfunctions) $\phi_r(x)$ as

$$w_{rel}(x,t) = \sum_{r=1}^{\infty} \phi_r(x)\eta_r(t) \qquad (3)$$

where the eigenfunctions of a cantilevered Euler–Bernoulli beam with a tip mass attachment can be expressed for the r-th vibration mode (of the undamped problem) as

$$\phi_r(x) = C_r\left[\cos\frac{\lambda_r}{L}x - \cosh\frac{\lambda_r}{L}x + s_r\left(\sin\frac{\lambda_r}{L}x - \sinh\frac{\lambda_r}{L}x\right)\right] \qquad (4)$$

Here, s_r is obtained from

$$s_r = \frac{\sin\lambda_r - \sinh\lambda_r + \lambda_r\frac{M_t}{mL}(\cos\lambda_r - \cosh\lambda_r)}{\cos\lambda_r + \cosh\lambda_r - \lambda_r\frac{M_t}{mL}(\sin\lambda_r - \sinh\lambda_r)} \qquad (5)$$

and C_r is a modal amplitude constant that is evaluated by normalizing the eigenfunctions according to either one of the following orthogonality conditions:

$$\int_0^L \phi_s(x)m\phi_r(x)\,\mathrm{d}x + \phi_s(L)M_t\phi_r(L) + \left[\frac{\mathrm{d}\phi_s(x)}{\mathrm{d}x}I_t\frac{\mathrm{d}\phi_r(x)}{\mathrm{d}x}\right]_{x=L}$$
$$= \delta_{rs}$$
$$\int_0^L \phi_s(x)D\frac{\mathrm{d}^4\phi_r(x)}{\mathrm{d}x^4}\,\mathrm{d}x - \left[\phi_s(x)D\frac{\mathrm{d}^3\phi_r(x)}{\mathrm{d}x^3}\right]_{x=L}$$
$$+ \left[\frac{\mathrm{d}\phi_s(x)}{\mathrm{d}x}D\frac{\mathrm{d}^2\phi_r(x)}{\mathrm{d}x^2}\right]_{x=L} = \omega_r^2\delta_{rs} \qquad (6)$$

Here, I_t is the mass moment of inertia of the tip mass M_t about the free end of the elastic beam and δ_{rs} is the Kronecker delta.[2] Furthermore, ω_r is the undamped natural frequency of the r-th vibration mode in the short-circuit conditions (i.e., $R_l \to 0$) given by

$$\omega_r = \lambda_r^2\sqrt{\frac{D}{mL^4}} \qquad (7)$$

where the eigenvalues of the system (λ_r for mode r) are obtained from the following transcendental equation:

$$1 + \cos\lambda\cos h\lambda + \lambda\frac{M_t}{mL}(\cos\lambda\sin h\lambda - \sin\lambda\cos h\lambda)$$
$$- \frac{\lambda^3 I_t}{mL^3}(\cosh\lambda\sin\lambda + \sinh\lambda\cos\lambda)$$
$$+ \frac{\lambda^4 M_t I_t}{m^2 L^4}(1 - \cos\lambda\cosh\lambda) = 0 \qquad (8)$$

The electromechanically coupled ordinary differential equations in the modal coordinates can be given by the following equations (Erturk and Inman, 2009):

$$\frac{\mathrm{d}^2\eta_r(t)}{\mathrm{d}t^2} + 2\zeta_r\omega_r\frac{\mathrm{d}\eta_r(t)}{\mathrm{d}t} + \omega_r^2\eta_r(t) - \tilde{\theta}_r v(t) = \sigma_r a(t) \qquad (9)$$

$$C_p^{eq}\frac{\mathrm{d}v(t)}{\mathrm{d}t} + \frac{v(t)}{R_l} + \sum_{r=1}^{\infty}\tilde{\theta}_r\frac{\mathrm{d}\eta_r(t)}{\mathrm{d}t} = 0 \qquad (10)$$

where ζ_r is the modal mechanical damping ratio, $\tilde{\theta}_r$ is the modal electromechanical coupling ($\tilde{\theta}_r$ and C_p^{eq} are read from Table 1 depending on the series or parallel connection of the piezoceramic layers), and σ_r is the modal forcing term expressed as

Table 1. Modal electromechanical coupling and equivalent capacitance of a bimorph energy harvester for the series and parallel connections of the piezoceramic layers

	Series connection	Parallel connection
$\tilde{\theta}_r$	$\bar{e}_{31}bh_{pc}\frac{\mathrm{d}\phi_r(x)}{\mathrm{d}x}\Big|_{x=L}$	$2\bar{e}_{31}bh_{pc}\frac{\mathrm{d}\phi_r(x)}{\mathrm{d}x}\Big|_{x=L}$
C_p^{eq}	$\frac{\bar{\varepsilon}_{33}^S bL}{2h_p}$	$\frac{2\bar{\varepsilon}_{33}^S bL}{h_p}$

$$\sigma_r = -m \int_0^L \phi_r(x)\mathrm{d}x - \mathrm{M}_t\phi_r(L) \qquad (11)$$

In Table 1, for a beam-like thin cantilever, the plane-stress piezoelectric stress constant $\bar{e}_{31}$ can be given in terms of the more commonly used piezoelectric strain constant d_{31} as $\bar{e}_{31} = d_{31}/s_{11}^E$ (where s_{11}^E is the elastic compliance at constant electric field) and the plane-stress permittivity constant at constant strain is $\bar{\varepsilon}_{33}^s = \varepsilon_{33}^T - d_{31}^2/s_{11}^E$ (where ε_{33}^T is the permittivity component at constant stress). Note that, in Figure 1, the directions 1 and 3 are coincident with the directions x and z, respectively.

Steady-State Response to Harmonic Base Acceleration

If the base acceleration is harmonic of the form $a(t) = A_0 e^{j\omega t}$ (where A_0 is the base acceleration amplitude, ω is the excitation frequency, and j is the unit imaginary number), the steady-state analytical solution for the voltage-to-base acceleration frequency response function (FRF) is obtained from Equations (9) and (10) as follows:

$$\alpha(\omega) = \frac{v(t)}{A_0 e^{j\omega t}} = \frac{\displaystyle\sum_{r=1}^{\infty} \frac{-j\omega\tilde{\theta}_r\sigma_r}{\omega_r^2 - \omega^2 + j2\zeta_r\omega_r\omega}}{\displaystyle\frac{1}{R_l} + j\omega C_p^{eq} + \sum_{r=1}^{\infty} \frac{j\omega\tilde{\theta}_r^2}{\omega_r^2 - \omega^2 + j2\zeta_r\omega_r\omega}} \qquad (12)$$

and the steady-state vibration response-to-base acceleration FRF is

$$\beta(\omega, x) = \frac{w_{rel}(x,t)}{A_0 e^{j\omega t}}$$
$$= \sum_{r=1}^{\infty} \left[\left(\sigma_r - \tilde{\theta}_r \frac{\displaystyle\sum_{r=1}^{\infty} \frac{j\omega\tilde{\theta}_r\sigma_r}{\omega_r^2 - \omega^2 + j2\zeta_r\omega_r\omega}}{\displaystyle\frac{1}{R_l} + j\omega C_p^{eq} + \sum_{r=1}^{\infty} \frac{j\omega\tilde{\theta}_r^2}{\omega_r^2 - \omega^2 + j2\zeta_r\omega_r\omega}} \right) \frac{\phi_r(x)}{\omega_r^2 - \omega^2 + j2\zeta_r\omega_r\omega} \right] \qquad (13)$$

For excitations close to a natural frequency, that is, $\omega \approx \omega_r$, the multimode Equations (12) and (13) reduce to the following single-mode equations:

$$\hat{\alpha}(\omega) = \frac{\hat{v}(t)}{A_0 e^{j\omega t}}$$
$$= \frac{-j\omega R_l\tilde{\theta}_r\sigma_r}{(1 + j\omega R_l C_p^{eq})(\omega_r^2 - \omega^2 + j2\zeta_r\omega_r\omega) + j\omega R_l\tilde{\theta}_r^2} \qquad (14)$$

$$\hat{\beta}(\omega, x) = \frac{\hat{w}_{rel}(x,t)}{A_0 e^{j\omega t}}$$
$$= \frac{(1 + j\omega R_l C_p^{eq})\sigma_r\phi_r(x)}{(1 + j\omega R_l C_p^{eq})(\omega_r^2 - \omega^2 + j2\zeta_r\omega_r\omega) + j\omega R_l\tilde{\theta}_r^2} \qquad (15)$$

where $r = 1$ for the frequently investigated case of excitation around the fundamental vibration mode to obtain the largest power output.

Response to Generalized Base Acceleration

In order to formulate the problem of piezoelectric energy harvesting for generalized or transient acceleration inputs, Equations (9) and (10) can be given in the first-order form as

$$\left\{ \begin{array}{c} \dot{u}_r^{(1)} \\ \dot{u}_r^{(2)} \\ \dot{u}^{(3)} \end{array} \right\} = \left\{ \begin{array}{c} u_r^{(2)} \\ -2\zeta_r\omega_r u_r^{(2)} - \omega_r^2 u_r^{(1)} + \tilde{\theta}_r u^{(3)} + \sigma_r a(t) \\ \frac{-u^{(3)}}{R_l C_p^{eq}} - \displaystyle\sum_{r=1}^{\infty} \frac{\tilde{\theta}_r u_r^{(2)}}{C_p^{eq}} \end{array} \right\} \qquad (16)$$

where the overdot represents differentiation with respect to time while the state variables are

$$u_r^{(1)}(t) = \eta_r(t), \ \ u_r^{(2)}(t) = \frac{\mathrm{d}\eta_r(t)}{\mathrm{d}t}, \ \ u^{(3)}(t) = v(t) \qquad (17)$$

Note that the energy harvester beam has infinitely many vibration modes (i.e., $r = 1, 2, \ldots$). Depending on the frequency content of the base acceleration input and the modal frequencies of the harvester beam, it is sufficient to consider a few vibration modes (say N modes), hence the dimension of the first-order representation reduces to $2N + 1$.

If the initial displacement and velocity distributions of the harvester beam are denoted by $\kappa(x)$ and $\mu(x)$, respectively, and the initial voltage across the load is v_0, the following summarizes the initial conditions in the physical coordinates:

$$w_{rel}(x, 0) = \kappa(x), \ \ \left. \frac{\partial w_{rel}(x,t)}{\partial t} \right|_{t=0} = \mu(x), \ \ v(0) = v_0 \qquad (18)$$

The first orthogonality condition given by Equation (6) can be used to obtain the initial conditions for two of the state variables as

$$u_r^{(1)}(0) = \eta_r(0)$$
$$= \int_0^L \kappa(x)m\phi_r(x)\mathrm{d}x + \kappa(L)M_t\phi_r(L) + \left[\frac{\mathrm{d}\kappa(x)}{\mathrm{d}x} I_t \frac{\mathrm{d}\phi_r(x)}{\mathrm{d}x} \right]_{x=L} \qquad (19)$$

$$u_r^{(2)}(0) = \left. \frac{\mathrm{d}\eta_r(t)}{\mathrm{d}t} \right|_{t=0}$$
$$= \int_0^L \mu(x)m\phi_r(x)\mathrm{d}x + \mu(L)M_t\phi_r(L) + \left[\frac{\mathrm{d}\mu(x)}{\mathrm{d}x} I_t \frac{\mathrm{d}\phi_r(x)}{\mathrm{d}x} \right]_{x=L} \qquad (20)$$

and the initial condition for the third state variable is simply

$$u^{(3)}(0) = v(0) = v_0 \quad (21)$$

Having the first-order form of the electromechanical equations and the initial conditions of the state variables (the initial conditions are often zero), an appropriate ordinary differential equation solver can be employed to solve for the response to arbitrary acceleration inputs.

Response to Broadband Base Acceleration of White Noise Type

For a linear random process (Newland, 1993), if the power spectral density (PSD) of the base acceleration $a(t)$ is $S_a(\omega)$, the PSD of the voltage output is obtained from

$$S_v(\omega) = |\alpha(\omega)|^2 S_a(\omega) \quad (22)$$

where $\alpha(\omega)$ is given by Equation (12). The inverse Fourier transform of the PSD of the voltage output is its autocorrelation function:

$$R_v(\tau) = \int_{-\infty}^{\infty} S_v(\omega) e^{j\omega\tau} d\omega = \int_{-\infty}^{\infty} |\alpha(\omega)|^2 S_a(\omega) e^{j\omega\tau} d\omega \quad (23)$$

For the case of ideal white noise excitation (Newland, 1993), the input PSD covers the entire frequency band with constant amplitude, yielding

$$R_v(\tau) = S_0 \int_{-\infty}^{\infty} |\alpha(\omega)|^2 e^{j\omega\tau} d\omega \quad (24)$$

where S_0 is the constant PSD of the base acceleration $a(t)$.

The mean square value of the voltage output is related to its autocorrelation function based on the following expression:

$$E[v^2(t)] = R_v(0) = \int_{-\infty}^{\infty} |\alpha(\omega)|^2 S_a(\omega) d\omega = S_0 \int_{-\infty}^{\infty} |\alpha(\omega)|^2 d\omega \quad (25)$$

where the ideal white noise spectral density is substituted. Recalling that the electrical power output is simply $v^2(t)/R_l$, the expected value of the power output becomes

$$E[P(t)] = \frac{S_0}{R_l} \int_{-\infty}^{\infty} |\alpha(\omega)|^2 d\omega \quad (26)$$

Therefore, the exact analytical solution for the expected value of the power output is obtained from

$$E[P(t)] = \frac{S_0}{R_l} \int_{-\infty}^{\infty} \left| \frac{\sum_{r=1}^{\infty} \frac{-j\omega\tilde{\theta}_r \sigma_r}{\omega_r^2 - \omega^2 + j2\zeta_r \omega_r \omega}}{\frac{1}{R_l} + j\omega C_p^{eq} + \sum_{r=1}^{\infty} \frac{j\omega\tilde{\theta}_r^2}{\omega_r^2 - \omega^2 + j2\zeta_r \omega_r \omega}} \right|^2 d\omega \quad (27)$$

which can be simplified dramatically by considering only the fundamental vibration mode (based on the reasoning that the highest energy is around the first natural frequency):

$$E[\hat{P}(t)] = \frac{S_0}{R_l} \int_{-\infty}^{\infty} \left| \frac{-j\omega R_l \tilde{\theta}_1 \sigma_1}{(1 + j\omega R_l C_p^{eq})(\omega_1^2 - \omega^2 + j2\zeta_1 \omega_1 \omega) + j\omega R_l \tilde{\theta}_1^2} \right|^2 d\omega \quad (28)$$

Using the integration relations in Newland's appendix (Newland, 1993) gives

$$E[\hat{P}(t)] = \frac{\pi S_0 R_l \tilde{\theta}_1^2 \sigma_1^2}{R_l \tilde{\theta}_1^2 + 2\zeta_1 \omega_1 \left[(1 + R_l^2 \tilde{\theta}_1^2 C_p^{eq}) + (2\zeta_1 + R_l C_p^{eq} \omega_1)(R_l C_p^{eq} \omega_1) \right]} \quad (29)$$

which is analogous to the lumped parameter derivations given by Halvorsen (2008) and Adhikari et al. (2009).

Piezoelectric Energy Harvesting from Moving Load Excitation

The problem of piezoelectric power generation from moving load excitation is formulated for two scenarios by focusing on a slender bridge[3] configuration (for possible applications to high-span highway bridges). The problems considered in the following are (1) energy harvesting from the vibrations of a piezoelectric cantilever located at an arbitrary point on the bridge and (2) energy harvesting using a thin piezoceramic patch covering an arbitrary region on the bridge.

Cantilevered Piezoelectric Energy Harvester Located on a Slender Bridge

The uniform slender bridge shown in Figure 2 is under the excitation of a transversely applied constant-amplitude point load P (representing a vehicle) moving at a constant speed $\bar{v}$. The equation of motion governing the vibrations of the bridge is

$$\bar{D} \frac{\partial^4 \bar{w}(\bar{x}, t)}{\partial \bar{x}^4} + \bar{c}_s \frac{\partial^5 \bar{w}(\bar{x}, t)}{\partial \bar{x}^4 \partial t} + \bar{c}_m \frac{\partial \bar{w}(\bar{x}, t)}{\partial t} + \bar{m} \frac{\partial^2 \bar{w}(\bar{x}, t)}{\partial t^2} = P\delta(\bar{x} - \bar{v}t) \quad (30)$$

where $\bar{w}(\bar{x}, t)$ is the vibration response of the bridge (transverse displacement of the neutral axis at position $\bar{x}$ and time t), $\bar{D}$ is the bending stiffness, $\bar{m}$ is the
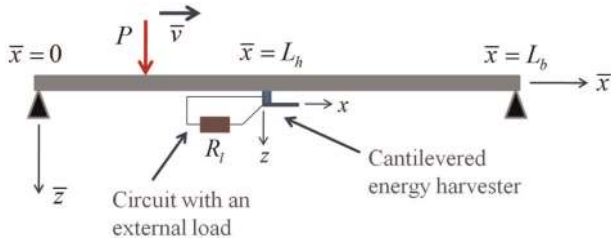
Figure 2. Schematic of the moving load problem for a slender bridge with a cantilevered bimorph energy harvester (the size of the cantilever is exaggerated).

mass per length, $\bar{c}_s$ and $\bar{c}_m$ represent the stiffness proportional and mass proportional damping components, respectively, and $\delta(\bar{x})$ is the Dirac delta function. The reference frame of the cantilevered piezoelectric energy harvester located at $\bar{x} = L_h$ is the xz-frame (as in Figure 1) while the reference frame of the bridge is the $\bar{x}\bar{z}$-frame as shown in Figure 2 (therefore, x is the axial position on the harvester beam, whereas $\bar{x}$ is the axial position on the bridge). The governing electromechanical equations of the cantilevered bimorph energy harvester located on the bridge are given by Equations (1) and (2). The basic assumption in the following derivation is that the effect of the small harvester beam and its dynamics on the bridge is negligible. As the load travels on the bridge, the energy harvester is excited and electrical power is generated but the bridge dynamics is not affected; therefore, no electrical term exists in Equation (30). The structural dynamics of the energy harvester beam can be affected by piezoelectric power generation (Lesieutre et al., 2004), which is taken into account in Equations (1) and (2).

The systematic approach is, therefore, to solve for the vibration response of the bridge to use it as the excitation term in the governing equations of the energy harvester. The base acceleration of the energy harvester in the first-order representation given by Equation (16) is therefore due to the vibration response of the bridge at $\bar{x} = L_h$ through

$$a(t) = \left. \frac{\partial^2 \bar{w}(\bar{x}, t)}{\partial t^2} \right|_{\bar{x} = L_h} \tag{31}$$

The following derivation provides the solution of $\bar{w}(\bar{x}, t)$ for $0 \leq t \leq T$ (where $T = L_b / \bar{v}$ is the time of traverse of the moving load over the bridge), so that it can be used in the electromechanical equations of the energy harvester to obtain the electrical response for a given resistive electrical load and a mechanical moving load. The analytical treatment of the undamped version of Equation (30) can be found in many texts and articles (Fryba, 1972; Olsson, 1991; Rao, 2007; Timoshenko et al., 1974). The damped

problem results in rather lengthy expressions but the analytical modal analysis procedure is applicable since the system is assumed to be proportionally damped.

The vibratory response of the slender bridge can be expressed as

$$\bar{w}(\bar{x}, t) = \sum_{r=1}^{\infty} \bar{\phi}_r(\bar{x}) \bar{\eta}_r(t) \tag{32}$$

where $\bar{\phi}_r(\bar{x})$ is the mass-normalized eigenfunction and $\bar{\eta}_r(t)$ is the modal coordinate for the r-th vibration mode of the bridge. The mass-normalized eigenfunction for simple end conditions is

$$\bar{\phi}_r(\bar{x}) = \sqrt{\frac{2}{\bar{m}L_b}} \sin\left(\frac{r\pi\bar{x}}{L_b}\right) \tag{33}$$

Equation (33) satisfies the orthogonality conditions

$$\int_0^{L_b} \bar{\phi}_s(\bar{x})\bar{m}\bar{\phi}_r(\bar{x})\mathrm{d}\bar{x} = \delta_{rs}, \quad \int_0^{L_b} \bar{\phi}_s(\bar{x})\bar{D}\frac{\mathrm{d}^4\bar{\phi}_r(\bar{x})}{\mathrm{d}\bar{x}^4}\mathrm{d}\bar{x} = \bar{\omega}_r^2\delta_{rs} \tag{34}$$

where the undamped natural frequency for the r-th vibration mode of the bridge is

$$\bar{\omega}_r = (r\pi)^2 \sqrt{\frac{\bar{D}}{\bar{m}L_b^4}} \tag{35}$$

Following the standard modal analysis procedure (Meirovitch, 2001), the modal equation of motion is obtained as

$$\frac{\mathrm{d}^2\bar{\eta}_r(t)}{\mathrm{d}t^2} + 2\bar{\zeta}_r\bar{\omega}_r\frac{\mathrm{d}\bar{\eta}_r(t)}{\mathrm{d}t} + \bar{\omega}_r^2\bar{\eta}_r(t) = P\sqrt{\frac{2}{\bar{m}L_b}}\sin\left(\frac{r\pi\bar{v}t}{L_b}\right) \tag{36}$$

where $\bar{\zeta}_r$ is the modal mechanical damping ratio ($\bar{\zeta}_r = \bar{c}_s\bar{\omega}_r/2\bar{D} + \bar{c}_m/2\bar{m}\bar{\omega}_r$).

For zero initial conditions of the bridge (in terms of the displacement and velocity fields), the total solution to Equation (36) is obtained in view of the initial conditions and the orthogonality conditions as

$$\bar{\eta}_r(t) = F_r\left\{\sin\left(\frac{r\pi\bar{v}t}{L_b} - \varphi_r\right) + e^{-\bar{\xi}_r\bar{\omega}_r t}\right.$$
$$\left[\sin\varphi_r\cos\bar{\omega}_r t + \left(\bar{\xi}_r\sin\varphi_r - \frac{r\pi\bar{v}}{\bar{\omega}_r L_b}\cos\varphi_r\right)\sin\bar{\omega}_r t\right]\right\} \tag{37}$$

where

$$F_r = P\sqrt{\frac{2}{\bar{m}L_b\left\{\left[\bar{\omega}_r^2 - \left(\frac{r\pi\bar{v}}{L_b}\right)^2\right]^2 + \left(\frac{2\bar{\zeta}_r\bar{\omega}_r r\pi\bar{v}}{L_b}\right)^2\right\}}},$$

$$\varphi_r = \tan^{-1}\left(\frac{\frac{2\bar{\zeta}_r\bar{\omega}_r r\pi\bar{v}}{L_b}}{\bar{\omega}_r^2 - \left(\frac{r\pi\bar{v}}{L_b}\right)^2}\right) \quad (38)$$

The vibration response is then[4]

$$\bar{w}(\bar{x}, t) = \sum_{r=1}^{\infty} \bar{\phi}_r(\bar{x})F_r\left\{\sin\left(\frac{r\pi\bar{v}t}{L_b} - \varphi_r\right) + e^{-\bar{\xi}_r\bar{\omega}_r t}\right.$$
$$\left.\left[\sin\varphi_r\cos\bar{\omega}_r t + \left(\bar{\xi}_r\sin\varphi_r - \frac{r\pi\bar{v}}{\bar{\omega}_r L_b}\cos\varphi_r\right)\sin\bar{\omega}_r t\right]\right\} \quad (39)$$

Therefore, the acceleration input to the cantilevered energy harvester located at $\bar{x} = L_h$ is

$$a(t) = \sum_{r=1}^{\infty} \bar{\phi}_r(L_h)F_r\frac{d^2}{dt^2}\left\{\sin\left(\frac{r\pi\bar{v}t}{L_b} - \varphi_r\right) + e^{-\bar{\xi}_r\bar{\omega}_r t}\right.$$
$$\left.\left[\sin\varphi_r\cos\bar{\omega}_r t + \left(\bar{\xi}_r\sin\varphi_r - \frac{r\pi\bar{v}}{\bar{\omega}_r L_b}\cos\varphi_r\right)\sin\bar{\omega}_r t\right]\right\} \quad (40)$$

which can be further expanded after the application of the differentiation. The transverse acceleration given by Equation (40) is the input to the first-order representation of the energy harvester equations given by Equation (16).

The nature of the bridge response strongly depends on the speed of the moving load. Fryba (1972) normalizes the $\pi\bar{v}/L_b$ term with respect to the fundamental natural frequency of the bridge and defines the dimensionless parameter $\alpha = \pi\bar{v}/\bar{\omega}_1 L_b$. Olsson (1991) reports that $\alpha = 1$ typically corresponds to a vehicle speed of 400–1500 km/h depending on the structural flexibility of the bridge, defining a conservative upper limit for most practical purposes. For the fast vehicle speed of $\alpha = 1$, the midspan ($\bar{x} = L_b/2$) reaches its maximum deflection (implying a quarter cycle of vibration) after the vehicle exits the bridge (Olsson, 1991). Simulations given in Fryba (1972) show that the maximum dynamic deflection is obtained for $0.5 \leqslant \alpha \leqslant 0.7$. For large values of α, the deflection rapidly tends to zero, whereas it converges to the static deflection for low values of α.

Large-span highway bridges are usually lightly damped structures (Fryba, 1972). Moreover, if the vehicle speed satisfies $\alpha \ll 1$ (i.e., $\bar{v} \ll \bar{\omega}_1 L_b/\pi$), the response is dominated by the fundamental vibration mode of the bridge. Therefore, taking only the first term ($r = 1$) in the summation of Equation (39) due to low vehicle speed and setting $\bar{\xi}_1 \ll 1$ due to light damping of the bridge simplifies Equation (39) to

$$\bar{w}(\bar{x}, t) \cong \bar{\phi}_1(\bar{x})F_1\sin\frac{\pi\bar{v}t}{L_b} = \frac{2P}{\bar{m}\bar{\omega}_1^2 L_b}\sin\frac{\pi L_h}{L_b}\sin\frac{\pi\bar{v}t}{L_b} \quad (41)$$

Thus, the dynamic response of the bridge is reduced to simple harmonic motion as a first approximation. Consequently, the acceleration input to the cantilevered energy harvester is also harmonic due to

$$a(t) = \frac{\partial^2 \bar{w}(\bar{x}, t)}{\partial t^2}\bigg|_{\bar{x}=L_h} \cong \bar{\phi}_1(L_h)F_1\frac{d^2}{dt^2}\left(\sin\frac{\pi\bar{v}t}{L_b}\right)$$
$$= -\frac{2P\pi^2\bar{v}^2}{\bar{m}\bar{\omega}_1^2 L_b^3}\sin\frac{\pi L_h}{L_b}\sin\frac{\pi\bar{v}t}{L_b} \quad (42)$$

Hence, the harmonic solution of the piezoelectric energy harvester equations can be used for designing the cantilever. If the typical vehicle speed is known along with the span length, the fundamental resonance frequency of the cantilever should be chosen as $\pi\bar{v}/L_b$. Moreover, the parameters of the energy harvester can be optimized (Erturk and Inman, 2011b; Renno et al., 2009) based on the harmonic solution at this frequency since the optimal parameters (such as the optimal electrical load) strongly depend on the excitation frequency (but they do not depend on the base acceleration amplitude in the linear energy harvesting problem). For a set of vehicle speed and span length combinations, Figure 3 shows the variation of the excitation frequency of the cantilever obtained from $\omega = \pi\bar{v}/L_b$. Note that the form of Equation (42) is strictly for $\bar{v} \ll \bar{\omega}_1 L_b/\pi$ and $\bar{\xi}_1 \ll 1$ (therefore, the frequencies shown in Figure 3 are the single-harmonic excitation frequencies of the energy harvester only for this condition). That is, the assumption is that the fundamental natural frequency of the bridge is much higher than the vehicle-induced frequency. If the fundamental natural frequency of the bridge is such that the vehicle-induced frequency ($\omega = \pi\bar{v}/L_b$) interacts with it (or with the frequencies of higher modes), the general form of Equation (40) should be used.

The voltage response of the piezoelectric energy harvester due to Equations (1) and (2) or due to Equation (16) is proportional to the excitation amplitude. Ideally, the cantilevered energy harvester should be located at
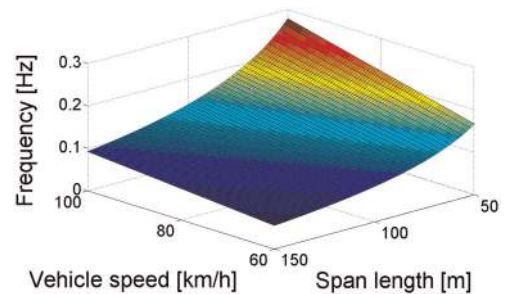

Figure 3. Variation of the vehicle-induced frequency with vehicle speed and span length.

the position of the maximum dynamic response on the bridge. The position of the maximum dynamic response is related to the eigenfunction expression given by Equation (33). Expectedly, if the response of the bridge is dominated by the fundamental vibration mode (for low vehicle speeds), the ideal location is obtained from Equation (33) as the midspan of the bridge ($\bar{x} = L_b/2$). If the bridge response is dominated by higher vibration modes, one should avoid locating the energy harvester at the nodal positions of the respective eigenfunctions and use the antinodal positions if the typical speeds in the traffic (therefore, the excitation frequencies and the expected mode shapes) are known.

Thin Piezoceramic Patch Covering a Region on a Slender Bridge

In many cases, vehicle-induced frequencies as well as bridge natural frequencies can be too low to excite a relatively stiff energy-harvesting cantilever effectively unless the cantilever is designed to be structurally very flexible. An alternative approach is presented in this section to harvest piezoelectric energy without using the cantilevered configuration. The slender bridge shown in Figure 4 has a piezoceramic patch covering the region $L_{h1} \leqslant \bar{x} \leqslant L_{h2}$ for harvesting energy from the vibrations induced by the moving load. The perfectly conductive electrodes covering the transverse faces of the patch are connected to an external resistive load. For the typical dimensions of commercially available piezoceramics, the patch length is much smaller than the length of the bridge, that is, $(L_{h2} - L_{h1}) \ll L_b$. However, several of such patches can be combined to generate usable electrical power from the dynamic strain induced on the surface by the moving load. The aim of this section is to relate the dynamic surface strain of the bridge (which is a function of the moving load) to the electrical output of the piezoceramic across a given resistive electrical load. It is reasonable to assume that the dynamics of the bridge are not affected by piezoelectric power generation. Therefore, the governing dynamic equation of the slender bridge and its vibration response are given by Equations (30) and (39), respectively.
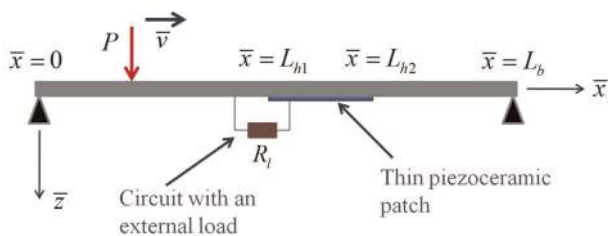

Figure 4. Schematic of the moving load problem for a slender bridge with a thin piezoceramic patch covering a region (the size of the patch is exaggerated).

As the admittance of the external circuit with a resistor is $1/R_l$, the integral form of Gauss's law leads to

$$\frac{\mathrm{d}}{\mathrm{d}t}\left(\int_A \mathbf{D} \cdot \mathbf{n}\mathrm{d}A\right) = \frac{v(t)}{R_l} \quad (43)$$

where $v(t)$ is the voltage across the resistive load, $\mathbf{D}$ is the vector of electric displacement components, $\mathbf{n}$ is the unit outward normal, and the integration is performed over the electrode area A of the piezoceramic patch.

For one-dimensional strain fluctuations, the electric displacement component in the thickness direction of the patch is

$$D_3 = \bar{e}_{31}S_1 + \bar{\varepsilon}_{33}^S E_3 \quad (44)$$

where D_3 is the electric displacement component, E_3 is the electric field component, S_1 is the longitudinal strain component while the piezoelectric stress constant ($\bar{e}_{31}$) and the permittivity component ($\bar{\varepsilon}_{33}^S$) are as defined earlier (the directions 1 and 3 are coincident with the directions $\bar{x}$ and $\bar{z}$ in Figure 4).

Since the electrodes are perpendicular to the transverse direction, the only nonzero component of the inner product in Equation (43) is due to Equation (44). After expressing the mechanical strain in the piezoceramic in terms of the curvature of the bridge and the electric field in terms of the voltage across the load, the governing circuit equation is obtained from Equation (43) as

$$C_p \frac{\mathrm{d}v(t)}{\mathrm{d}t} + \frac{v(t)}{R_l} = -\bar{e}_{31}h_{pc}b_p \int_{L_{h1}}^{L_{h2}} \frac{\partial^3 \bar{w}(\bar{x}, t)}{\partial \bar{x}^2 \partial t} \mathrm{d}\bar{x} \quad (45)$$

where b_p is the width of the piezoceramic (equal to the width of the electrodes), h_{pc} is the distance from the neutral axis of the bridge to the center of the piezoceramic patch, $\bar{e}_{31}$ is the effective (plane-stress) piezoelectric stress constant, and C_p is the capacitance of the piezoceramic patch ($C_p = \bar{\varepsilon}_{33}^S b_p (L_{h2} - L_{h1})/h_p$, where h_p is the thickness of the piezoceramic).

Substituting the response form given by Equation (32) in Equation (45) gives

$$\frac{\mathrm{d}v(t)}{\mathrm{d}t} + \frac{v(t)}{\tau} = \sum_{r=1}^{\infty} \psi_r \frac{\mathrm{d}\bar{\eta}_r(t)}{\mathrm{d}t} \quad (46)$$

where $\bar{\eta}_r(t)$ is given by Equation (37), τ is the time constant of the circuit given by $\tau = R_l C_p$, and the modal electromechanical coupling is

$$\psi_r = -\frac{\bar{e}_{31}h_{pc}b_p}{C_p}\int_{L_{h1}}^{L_{h2}} \frac{\mathrm{d}^2\bar{\phi}_r(\bar{x})}{\mathrm{d}\bar{x}^2}\mathrm{d}\bar{x} = -\frac{\bar{e}_{31}h_{pc}b_p}{C_p}\frac{\mathrm{d}\bar{\phi}_r(\bar{x})}{\mathrm{d}\bar{x}}\bigg|_{\bar{x}=L_{h1}}^{\bar{x}=L_{h2}}$$

$$(47)$$

Equation (46) can be solved by using the integrating factor $e^{t/\tau}$, yielding

$$v(t) = e^{\frac{-t}{\tau}} \int e^{\frac{t}{\tau}} \sum_{r=1}^{\infty} \psi_r \frac{\mathrm{d}\bar{\eta}_r(t)}{\mathrm{d}t} \mathrm{d}t \qquad (48)$$

where the initial voltage is assumed to be zero. Therefore, for the external resistive load R_l, the electrical power output is

$$P(t) = \frac{1}{R_l} \left[e^{\frac{-t}{\tau}} \int e^{\frac{t}{\tau}} \sum_{r=1}^{\infty} \psi_r \frac{\mathrm{d}\bar{\eta}_r(t)}{\mathrm{d}t} \mathrm{d}t \right]^2 \qquad (49)$$

The excitation of the piezoceramic patch (and hence, its electrical output) is proportional to the dynamic strain field induced over the region it covers. From Equation (47), the optimal region to cover is the region of maximum curvature, so that ψ_r is maximized for a given vibration mode r. Therefore, for vibrations with the fundamental mode of the bridge ($r = 1$), one should prefer covering the region $(L_b - L_p)/2 \leqslant \bar{x} \leqslant (L_b + L_p)/2$ (where L_p is the length of the patch). For vibrations with higher modes, covering the inflection points (strain nodes (Erturk et al., 2009b)) of the bridge with a single patch results in cancellation of the electrical output. Nevertheless, in practice, it is necessary to use several patches (due to their size limitations) for covering a significant region on the bridge and one simply needs to consider the phases of the electrical outputs before combining them in the circuit to avoid cancellations (Erturk et al., 2009b).

Piezoelectric Energy Harvesting from Local Strain Fluctuations

The derivation given in this section aims to express the power output due to the dynamic strain field induced in a small rectangular piezoceramic patch attached onto a vibrating host structure (Figure 5). Therefore, the problem considered here is a local and two-dimensional way of treating the problem of the previous section. The inputs in the following derivation are the dynamic strain components in two perpendicular directions
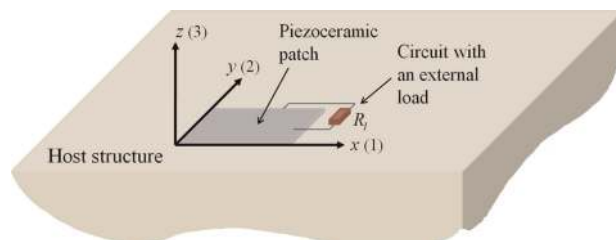

Figure 5. Rectangular thin piezoceramic patch attached onto a large civil engineering structure for power generation from two-dimensional surface strain fluctuations.

rather than the original source of the excitation (e.g., moving load, fluid–structure interaction). Hence, the generalized derivation covered here can be used for estimating the piezoelectric power output extracted from the surface strain energy of various engineering structures. The electromechanical response to generalized, harmonic, and random strain fluctuations are derived in the following section.

Response to Generalized Strain Fluctuations

In Figure 5, the dynamic loading condition (not shown) and the orientation of the rectangular thin piezoceramic patch are such that the patch is exposed to strain fluctuations in two perpendicular directions, such as the principal strain directions (Gere and Timoshenko, 1990). The perfectly conductive electrodes covering the upper and the lower faces of the piezoceramic patch are connected to a resistive electrical load. As in the moving load problem, it is assumed that the effect of piezoelectric power generation on the dynamics of the large structure is negligible. Moreover, the piezoceramic patch is much thinner than the host structure and the bonding is perfect, so that the average strain distribution in the patch is similar to the strain distribution on the covered surface of the structure.

For the thin rectangular piezoceramic undergoing strain fluctuations in the x and y directions ((1) and (2) in Figure 5), the nonzero electric displacement component is expressed as

$$D_3 = \bar{e}_{31}S_1 + \bar{e}_{32}S_2 + \bar{\varepsilon}_{33}^S E_3 \qquad (50)$$

where S_1 and S_2 are the strain components,[5] E_3 is the electric field component while the plane-stress piezoelectric stress constants and the permittivity component for a thin piezoceramic plate are obtained by neglecting the transverse shear and thickness stress components as

$$\bar{e}_{31} = \bar{e}_{32} = \frac{d_{31}}{s_{11}^E + s_{12}^E}, \quad \bar{\varepsilon}_{33}^S = \varepsilon_{33}^T - \frac{2d_{31}^2}{s_{11}^E + s_{12}^E} \qquad (51)$$

Here, d_{31} is the piezoelectric strain constant, s_{11}^E and s_{12}^E are the elastic compliance components at constant electric field, and ε_{33}^T is the permittivity component at constant stress. In Equation (51), the symmetry of transverse isotropy about the z-axis is applied by assuming a poled piezoelectric ceramic. Hence, Equation (50) becomes

$$D_3 = \bar{e}_{31}(S_1 + S_2) + \bar{\varepsilon}_{33}^S E_3 \qquad (52)$$

If the voltage across the resistive load R_l is denoted by $v(t)$, Equation (43) leads to

$$\frac{\mathrm{d}v(t)}{\mathrm{d}t} + \frac{v(t)}{\tau} = \frac{\bar{e}_{31}}{C_p} \int_A \frac{\partial}{\partial t} [S_1(x, y, t) + S_2(x, y, t)] \mathrm{d}A \qquad (53)$$

where $\tau = R_l C_p$ is the time constant and $C_p = \bar{\varepsilon}_{33}^S A / h_p$ is the capacitance of the piezoceramic patch (where h_p is its thickness and A is the electrode area).

For the space-dependent strain components $S_1(x, y, t)$ and $S_2(x, y, t)$, the solution of the voltage response is

$$v(t) = \frac{\bar{e}_{31}}{C_p} e^{\frac{-t}{\tau}} \int e^{\frac{t}{\tau}} \left\{ \int_A \frac{\partial}{\partial t} [S_1(x, y, t) + S_2(x, y, t)] dA \right\} dt \quad (54)$$

and the power output is obtained from

$$P(t) = \frac{1}{R_l} \left\langle \frac{\bar{e}_{31}}{C_p} e^{\frac{-t}{\tau}} \int e^{\frac{t}{\tau}} \left\{ \int_A \frac{\partial}{\partial t} [S_1(x, y, t) + S_2(x, y, t)] dA \right\} dt \right\rangle^2 \quad (55)$$

In order to maximize the spatial integrand in Equation (55), one should avoid covering the inflection lines of the host surface (where the strain components change sign) with a single patch.

If the strain field in each direction of the piezoceramic patch is homogenous (so that $S_1(t)$ and $S_2(t)$ are space-independent), the right-hand side of Equation (53) is simplified to give

$$\frac{dv(t)}{dt} + \frac{v(t)}{\tau} = \frac{\bar{e}_{31} A}{C_p} \frac{d}{dt} [S_1(t) + S_2(t)] \quad (56)$$

yielding the power output of

$$P(t) = \frac{1}{R_l} \left\{ \frac{\bar{e}_{31} A}{C_p} e^{\frac{-t}{\tau}} \int e^{\frac{t}{\tau}} \frac{d}{dt} [S_1(t) + S_2(t)] dt \right\}^2 \quad (57)$$

Steady-State Response to Harmonic Strain Fluctuations

Consider the case where the dynamic strain components are harmonic in time at the same frequency:

$$S_1(t) = \tilde{S}_1 e^{j\omega t}, \ S_2(t) = \tilde{S}_2 e^{j\omega t} \quad (58)$$

where $\tilde{S}_1$ and $\tilde{S}_2$ are the strain values (which might be complex valued to account for a phase difference), ω is the excitation frequency, and j is the unit imaginary number. In practice, each of the strain components could also have a DC (static) component, which has no contribution to the alternating voltage output of the piezoceramic patch at steady state.

The steady-state voltage output is obtained from Equation (56) as

$$v(t) = j\omega \bar{e}_{31} A (\tilde{S}_1 + \tilde{S}_2) \left(j\omega C_p + \frac{1}{R_l} \right)^{-1} e^{j\omega t} \quad (59)$$

Hence the steady-state power amplitude is

$$P = \frac{\omega^2 \bar{e}_{31}^2 A^2 (\tilde{S}_1 + \tilde{S}_2)^2 R_l}{1 + \omega^2 R_l^2 C_p^2} \quad (60)$$

which can be used to find the optimal electrical load as

$$\left. \frac{\partial P}{\partial R_l} \right|_{R_l = R_l^{opt}} = 0 \rightarrow R_l^{opt} = \frac{1}{\omega C_p} \quad (61)$$

Therefore, the maximum power output is simply

$$P_{max} = P|_{R_l = R_l^{opt}} = \frac{\omega \bar{e}_{31}^2 A^2 (\tilde{S}_1 + \tilde{S}_2)^2}{2 C_p} \quad (62)$$

Response to Broadband Strain Fluctuations of White Noise Type

For harmonic strain fluctuations in two perpendicular directions, one can define the following electromechanical FRF using Equation (59):

$$\chi(\omega) = \frac{v(t)}{j\omega (\tilde{S}_1 + \tilde{S}_2) e^{j\omega t}} = \frac{\bar{e}_{31} A R_l}{1 + j\omega R_l C_p} \quad (63)$$

which is the frequency-domain transfer function that relates the harmonic voltage response to the harmonic strain-rate resultant at steady state.

If the PSD of the white noise-type strain-rate resultant is given by $S_s(\omega) = S_0$, after following steps similar to those given for the base excitation problem, the expected value of the power output can be obtained as

$$E[P(t)] = \frac{1}{R_l} \int_{-\infty}^{\infty} |\chi(\omega)|^2 S_s(\omega) d\omega$$

$$= \frac{S_0}{R_l} \int_{-\infty}^{\infty} \left| \frac{\bar{e}_{31} A R_l}{1 + j\omega R_l C_p} \right|^2 d\omega = \frac{S_0 \pi (\bar{e}_{31} A)^2}{C_p} \quad (64)$$

Remarkably, for an ideal white noise–type strain-rate resultant, the expected value of the electrical power output extracted from the piezoceramic patch does not depend on the external load resistance. The power output in both harmonic and white noise excitations is proportional to $\bar{e}_{31}^2 / C_p$ due to Equations (62) and (64), respectively (where $C_p \propto \bar{\varepsilon}_{33}^S$). Therefore, the piezoelectric material should be chosen to maximize $\bar{e}_{31}^2 / \bar{\varepsilon}_{33}^S$ for harvesting energy from surface strain fluctuations using a patch.

Strain Gage Measurements and Strain Transformations

In practice, it is useful to measure the strain levels on the surface of the host structure to estimate the power output using the foregoing derivations prior to bonding
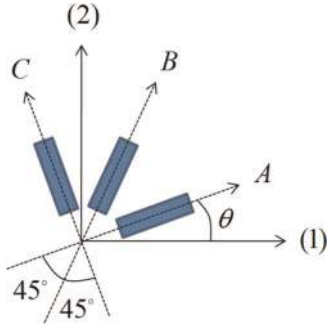
Figure 6. Schematic of a rectangular rosette configuration with gages A, B, and C and the principal strain directions 1 and 2.

a piezoceramic patch onto the host structure. The directions of principal strain components and the way they change in time (if they do) can also be checked. Usually, strain gage rosettes are employed for strain measurements and they consist of multiple gages oriented at a fixed angle with respect to each other. Figure 6 shows the schematic of a rectangular rosette configuration (where the angle between the gages is 45°). In general, at least three independent strain readings are required to define the two-dimensional state of strain assuming that no other information is available. The rectangular rosette configuration shown in Figure 6 gives three simultaneous strain measurements S_A, S_B, and S_C in A, B, and C directions, respectively. The directions of the principal strain components (S_1 and S_2) are denoted by 1 and 2.

Based on Mohr's circle (Gere and Timoshenko, 1990), the principal strain components are obtained from the following strain transformation:

$$S_{1,2} = \frac{S_A + S_C}{2} \pm \frac{1}{\sqrt{2}} \sqrt{(S_A - S_B)^2 + (S_B - S_C)^2} \quad (65)$$

and the angle between gage A and the direction of positive S_1 is

$$\theta = \frac{1}{2}\tan^{-1}\left(\frac{S_A - 2S_B + S_C}{S_A - S_C}\right) \quad (66)$$

Equations (65) and (66) give an idea regarding how the strain levels and the direction of principal strains change in time if the loading and structural conditions result in such variations. It is useful noticing from Equation (65) that

$$S_1 + S_2 = \frac{S_A + S_C}{2} + \frac{S_A + S_C}{2} = S_A + S_C \quad (67)$$

which implies that the strain resultant of two arbitrary but orthogonal directions ($S_A + S_C$) is equal to that of the principal strain directions ($S_1 + S_2$). Although determining the two-dimensional strain state on the surface requires three independent strain measurements, two orthogonal strain measurements are sufficient to estimate the resultant of the principal strain components and, therefore, the resulting power output for a rectangular patch oriented in the principal strain directions.

Case Study for Piezoelectric Energy Harvesting from Surface Strain Fluctuations

Analysis of a Piezoceramic Patch for Two-Dimensional Strain Fluctuations

This section analyzes a piezoceramic patch for piezoelectric power generation from surface strain fluctuations. The thin patch considered here is a $30 \times 30 \times 0.2$ mm^3 lead zirconate titanate PZT-5A square piezoceramic plate with $d_{31} = -171$ pm/V, $s_{11}^E = 16.4$ pm^2/N, $s_{12}^E = -5.74$ pm^2/N, $\varepsilon_{33}^T = 15.05$ nF/m (yielding $\bar{e}_{31} = -16$ C/m^2 and $\bar{\varepsilon}_{33}^S = 9.57$ nF/m). If two conductive electrodes of negligible thickness cover the opposite faces completely, the capacitance of the patch can be calculated as $C_p = 43$ nF. In the following simulations, it is assumed that the strain fluctuation is harmonic at the same frequency in both orthogonal strain directions, and the strain field in the patch is homogeneous. The input parameters required to predict the maximum power amplitude in Equation (62) are then the strain values ($\tilde{S}_1$ and $\tilde{S}_2$) and the frequency of harmonic fluctuation (ω).

Suppose that the strain components have the opposite sign at an arbitrary instant of time and they oscillate at 10 Hz. The peak power amplitudes for different combinations of $\tilde{S}_1$ and $\tilde{S}_2$ at this frequency are shown in Figure 7. In the simulations, $\tilde{S}_1$ takes values between 50 and 80 microstrain while $\tilde{S}_2$ takes values between -40 and -10 microstrain. It is known from Equation (62) that the important parameter is the resultant of these strain components given by $\tilde{S}_1 + \tilde{S}_2$. The maximum power output obtained for the resultant of 80 and -10 microstrain is 0.745 mW, whereas the minimum power output of 15.2 μW is obtained for the resultant of 50 and -40 microstrain. Since the frequency is fixed at 10 Hz, the matched (optimal) resistance of all combinations in Figure 7 is 369.7 kΩ.

The peak power amplitudes are plotted in Figure 8(a) for various strain resultant and frequency combinations while the optimal resistive loads of these combinations are plotted in Figure 8(b). For a fixed excitation frequency, the power output depends on the strain resultant quadratically, whereas for a fixed strain resultant, the power output changes with frequency linearly. The maximum power output of 0.951 mW is obtained in Figure 8(a) for a 50 microstrain resultant at 25 Hz frequency using this 9 cm^2 piezoceramic patch of 0.2 mm thickness. Note that the matched resistance grows dramatically at low frequencies (Figure 8(b))
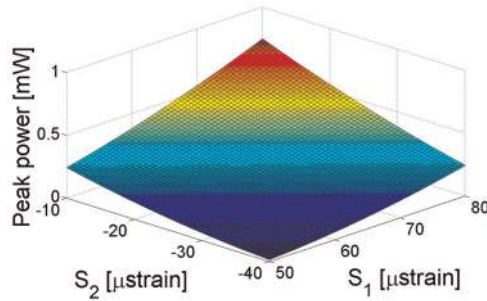
Figure 7. Variation of the peak power amplitude for different combinations of the principal strain components at 10 Hz.

since it is inversely proportional to the excitation frequency due to Equation (61).

Discussion Based on the Strain Gage Measurements for a Steel Multigirder Bridge

The dynamic strain measurements taken on the steel multigirder bridge shown in Figure 9(a) are briefly discussed to estimate the maximum piezoelectric power that can be generated using the patch studied in the previous section. The strain measurements were taken at a location on the bridge by using a rectangular rosette strain gage configuration (Figure 6). Figure 9(b) displays the strain measurements recorded at the point of interest with a sampling frequency of 82.6 Hz. The orientations of the gages A, B, and C can be found in Figure 6.

The raw strain data shown in Figure 9(b) are used in Equation (65) and the dynamic principal strain components shown in Figure 10(a) are obtained. A close-up view of the principal strain components is shown in Figure 10(b) at an arbitrary instant of time. Note that one component oscillates around a positive static value (static tension) whereas the other one oscillates around a negative static value (static compression). It is observed through fast Fourier transform (FFT)

analysis that a major harmonic exists at approximately 22.6 Hz in both components.

Recall from Equation (67) that the strain resultant $S_1 + S_2$ is identical to the resultant $S_A + S_C$. Figures 11(a) and (b) shows this strain resultant for the entire time history and for an arbitrary instant of time, respectively. Figure 11(b) also includes a single harmonic history of 20 microstrain amplitude at 22.6 Hz as a first approximation. If the dynamic behavior of the strain resultant can be approximated as a harmonic strain fluctuation of ± 20 microstrain at 22.6 Hz, the peak power amplitude is estimated from Figure 8(a) as 0.138 mW. Assuming homogeneous strain behavior in the small region and combining seven of such patches, one can reach milli-Watt level instantaneous power output based on this first approximation.

Summary and Conclusion

Civil infrastructure systems provide unique and critical application platforms for vibration-based energy harvesting. In particular, the state-of-the-art wireless and battery-powered sensor networks used for structural health monitoring can be made self-powered if sufficient vibrational energy is available in their environment. Among other transduction mechanisms used for vibration-to-electricity conversion, piezoelectric transduction has been most heavily researched in the last few years due to the ease of application and large power density of piezoelectric materials. This article introduces analytical derivations combining some of the fundamental civil engineering problems with the problem of piezoelectric energy harvesting.

The moving load problem for a slender bridge is visited for analytical formulation of two scenarios of piezoelectric energy harvesting. In the first scenario, a cantilevered piezoelectric energy harvester is located at an arbitrary position on the bridge. The vibratory response of the bridge caused by the moving load creates the excitation input to the generalized cantilevered
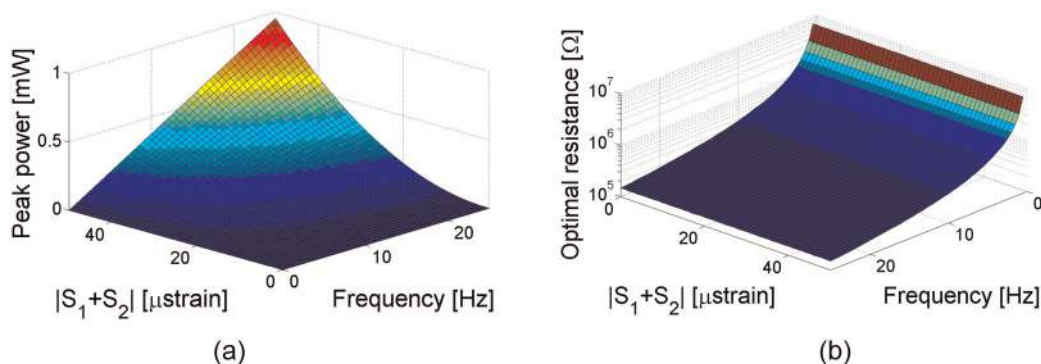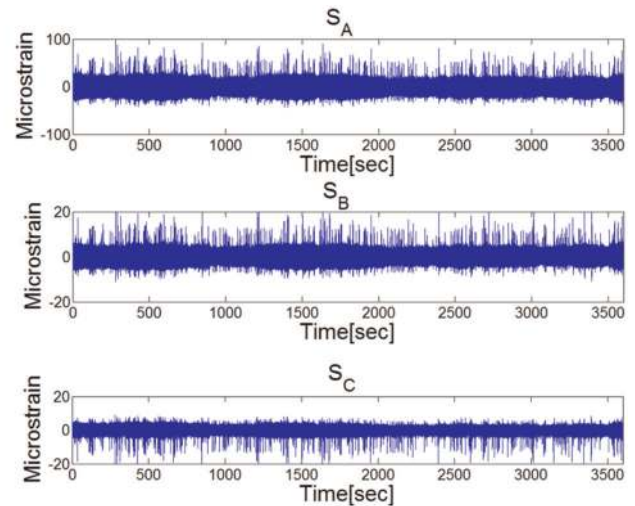

Figure 8. Variations of (a) the maximum power amplitude and (b) the optimal resistance values for different combinations of the strain resultant and the excitation frequency.
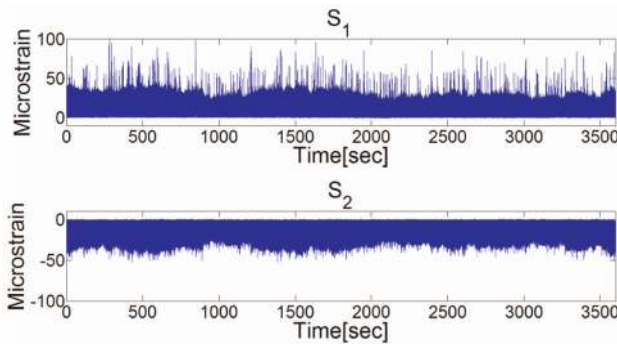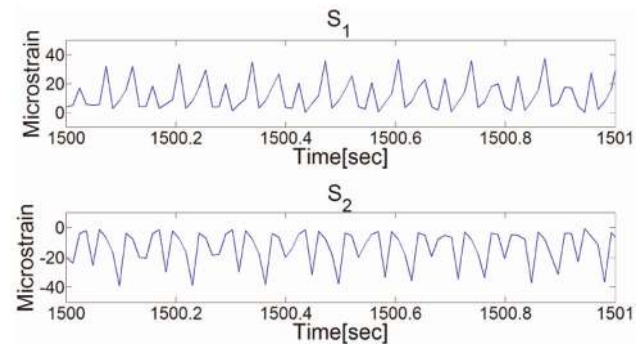
Figure 9. (a) The 3-span steel continuous curved multigirder bridge in Roanoke, Virginia, (span length: 33 m) and (b) the measured strain components at a point on the bridge using a rectangular rosette strain gage (see Figure 6 for the arrangement of gages A, B, and C).

Figure 10. Dynamic principal strain components: (a) the entire time history and (b) a close-up view at an arbitrary instant of time.

energy harvester equations covered in this article. Typical vehicle-induced frequencies and fundamental natural frequencies of slender bridges can be very low and the piezoelectric cantilever should be designed to have a very low fundamental natural frequency. As an alternative to using the cantilevered energy harvester configuration, a certain region on the bridge is covered with a piezoceramic patch in the second scenario. The piezoelectric power delivered from the patch to the electrical load is related to the moving load excitation based on the analytical electromechanical formulation.

Following the moving load excitation, the focus is placed on formulating the problem of piezoelectric energy harvesting from two-dimensional surface strain fluctuations of large structures. For the orthogonal strain fluctuations of a rectangular piezoceramic patch, analytical expressions of the electrical power output are obtained considering generalized, harmonic, and white noise excitations. It is shown using the model developed here that a $30\times30\times0.2\,\text{mm}^3$ piezoceramic patch can generate about 1 mW power for the dynamic orthogonal strain resultant of 50 microstrain at 25 Hz. An additional discussion is provided based on the dynamic strain measurements taken on the steel multigirder bridge. On the basis of a combination of the theoretical analysis and the field measurements, it is predicted that milli-Watt strain level can be obtained using a few patches for the relatively low strain levels measured on this nonslender bridge.

The derivations related to the fundamental moving load problem can be extended to other transduction mechanisms of vibration-based energy harvesting as well (e.g., electromagnetic transduction). However, piezoceramic patches offer a unique option for energy harvesting directly from the surface strain fluctuations of various civil infrastructure systems.
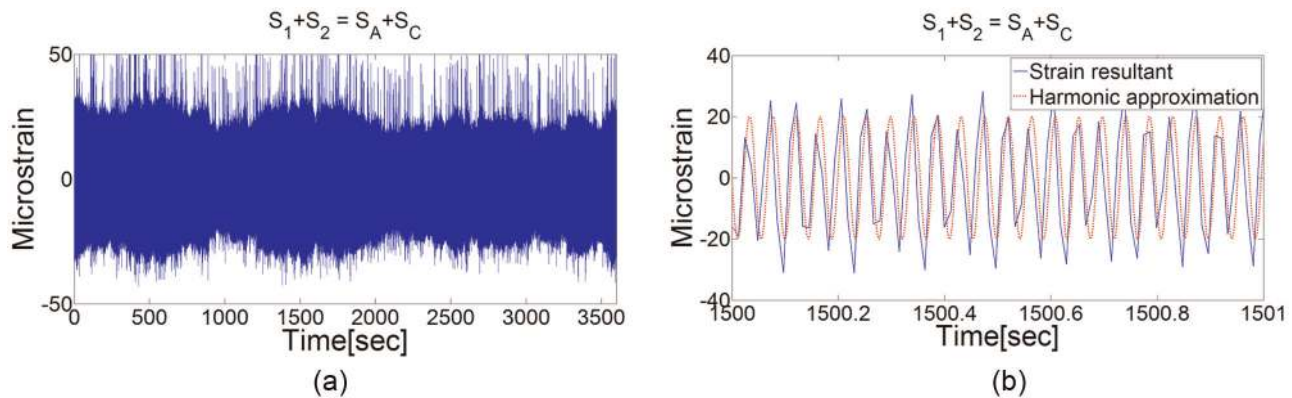
Figure 11. Resultant of the principal strain components: (a) the entire time history and (b) a close-up view at an arbitrary instant of time (along with the single harmonic approximation: 20 microstrain at 22.6 Hz).

Acknowledgment

Notes

1. Although combined dynamical systems (distributed parameter systems with lumped attachments) have certain limitations as far as the normal-mode assumption is concerned (Banks et al., 1998), as an engineering approximation, one can solve the undamped problem for $c_s I = c_a = 0$ (which is a normal-mode system (Caughey and O'Kelly, 1965)) and introduce modal viscous damping in the modal coordinates.
2. Note that this formulation (Erturk and Inman, 2009) accounts for the geometric information of the rigid tip mass attachment in case it does not behave like a point mass. The geometric information of the tip mass (e.g., prismatic or cylindrical) is included within the mass moment of inertia term (I_t) without loss of generality as a compact alternative to expanding it in terms of the geometry of the tip mass for a specific configuration (Kim et al., 2010). The mass moment of inertia of the tip mass should always be expressed in conjunction with the parallel axis theorem at the end of the elastic point where the boundary condition is written to be in agreement with the differential eigenvalue problem.
3. The term *bridge* is used (instead of beam) to avoid confusion with the energy harvester, which has a similar mechanical equation. The derivations apply to other slender structures exposed to moving loads.
4. In his book on the subject of moving loads, Fryba (1972) studies special cases regarding the speed of the load and the damping in the structure following his solution based on the Laplace–Carson integral transformation. The response expression is left in its general form in this article and the reader is referred to Fryba (1972) for an extensive discussion of special cases.
5. The derivations given here are for piezoelectric ceramics with conventional electrodes. Expectedly, fiber-based orthotropic piezoceramics with interdigitated electrodes, such as the active fiber composites and macro fiber composites (Williams et al., 2002), do not give any electrical output to strain fluctuations in the direction that is orthogonal to the longitudinal direction of fibers.

References

Adhikari S, Friswell MI and Inman DJ (2009) Piezoelectric energy harvesting from broadband random vibrations. *Smart Materials and Structures* 18: 115005.

Anton SR and Sodano HA (2007) A review of power harvesting using piezoelectric materials (2003–2006). *Smart Materials and Structures* 16: R1–R21.

Aureli M, Prince C, Porfiri M and Peterson SD (2010) Energy harvesting from base excitation of ionic polymer metal composites in fluid environments. *Smart Materials and Structures* 19: 015003.

Banks HT, Luo ZH, Bergman LA and Inman DJ (1998) On the existence of normal modes of damped discrete-continuous systems. *ASME Journal of Applied Mechanics* 65: 980–989.

Beeby SP, Tudor MJ and White NM (2006) Energy harvesting vibration sources for microsystems applications. *Measurement Science and Technology* 17: R175–R195.

Caughey TK and O'Kelly MEJ (1965) Classical normal modes in damped linear dynamic systems. *ASME Journal of Applied Mechanics* 32: 583–588.

Chiu Y and Tseng VFG (2008) A capacitive vibration-to-electricity energy converter with integrated mechanical switches. *Journal of Micromechanical and Microengineering* 18: 104004.

Cook-Chennault KA, Thambi N and Sastry AM (2008) Powering MEMS portable devices—A review of non-regenerative and regenerative power supply systems with emphasis on piezoelectric energy harvesting systems. *Smart Materials and Structures* 17: 043001.

Cottone F, Vocca H and Gammaitoni L (2009) Nonlinear energy harvesting. *Physical Review Letters* 102: 080601.

Daqaq MF (2010) Response of uni-modal duffing-type harvesters to random forced excitations. *Journal of Sound and Vibration* 329: 3621–3631.

Elvin NG and Elvin AA (2009) A general equivalent circuit model for piezoelectric generators. *Journal of Intelligent Material Systems and Structures* 20: 3–9.

Elvin NG, Elvin AA and Choi DH (2003) A self-powered damage detection sensor. *The Journal of Strain Analysis for Engineering Design* 38: 115–124.

Elvin NG, Lajnef N and Elvin AA (2006) Feasibility of structural monitoring with vibration powered sensors. *Smart Materials and Structures* 15: 977–986.

Erturk A, Hoffmann J and Inman DJ (2009a) A piezomagnetoelastic structure for broadband vibration energy harvesting. *Applied Physics Letters* 94: 254102.

Erturk A and Inman DJ (2009) An experimentally validated bimorph cantilever model for piezoelectric energy harvesting from base excitations. *Smart Materials and Structures* 18: 025009.

Erturk A and Inman DJ (2011a) Broadband piezoelectric power generator on high-energy orbits of the bistable duffing oscillator with electromechanical coupling. *Journal of Sound and Vibration* 330: 2339–2353.

Erturk A and Inman DJ (2011b) Parameter identification and optimization in piezoelectric energy harvesting: Analytical relations, asymptotic analyses, and experimental validations. *IMechE Journal of Systems and Control Engineering* 225: 485–496.

Erturk A, Tarazaga P, Farmer JR and Inman DJ (2009b) Effect of strain nodes and electrode configuration on piezoelectric energy harvesting from cantilevered beams. *ASME Journal of Vibration and Acoustics* 131: 011010.

Fryba L (1972) *Vibration of Solids and Structures under Moving Loads*. Groningen, the Netherlands: Noordhoff International Publishing.

Gere JM and Timoshenko SP (1990) *Mechanics of Materials*. Boston, MA: PWS-Kent Publishing Co.

Halvorsen E (2008) Energy harvesters driven by broadband random vibrations. *Journal of Microelectromechanical Systems* 17: 1061–1071.

Kim M, Hoegen M, Dugundji J and Wardle BL (2010) Modeling and experimental verification of proof mass effects on vibration energy harvester performance. *Smart Materials and Structures* 19: 045023.

Lesieutre GA, Ottman GK and Hofmann HF (2004) Damping as a result of piezoelectric energy harvesting. *Journal of Sound and Vibration* 269: 991–1001.

Litak G, Friswell MI and Adhikari S (2010) Magnetopiezoelastic energy harvesting driven by random excitations. *Applied Physics Letters* 96: 214103.

Mann BP and Sims ND (2009) Energy harvesting from the nonlinear oscillations of magnetic levitation. *Journal of Sound and Vibration* 319: 515–530.

Meirovitch L (2001) *Fundamentals of Vibrations*. New York: McGraw-Hill.

Newland DE (1993) *Random Vibrations, Spectral and Wavelet Analysis*. New York: John Wiley & Sons.

Olsson M (1991) On the fundamental moving load problem. *Journal of Sound and Vibration* 145: 299–307.

Ozevin D, Greve DW, Oppenheim IJ and Pessiki SP (2006) Resonant capacitive MEMS acoustic emission transducers. *Smart Materials and Structures* 15: 1863–1871.

Rao SS (2007) *Vibration of Continuous Systems*. Hoboken, NJ: John Wiley & Sons.

Renno JM, Daqaq MF and Inman DJ (2009) On the optimal energy harvesting from a vibration source. *Journal of Sound and Vibration* 320: 386–405.

Scruggs JT (2009) An optimal stochastic control theory for distributed energy harvesting networks. *Journal of Sound and Vibration* 320: 707–725.

Shigeishi M, Colombo S, Broughton KJ, Rutledge H, Batchelor AJ and Forde MC (2001) Acoustic emission to assess and monitor the integrity of bridges. *Construction and Building Materials* 15: 35–49.

Shu YC, Lien IC and Wu WJ (2007) An improved analysis of the SSHI interface in piezoelectric energy harvesting. *Smart Materials and Structures* 16: 2253–2264.

Sodano H, Park G and Inman DJ (2004) A review of power harvesting from vibration using piezoelectric materials. *Shock and Vibration Digest* 36: 197–205.

Stanton SC, Erturk A, Mann BP and Inman DJ (2010a) Resonant manifestation of intrinsic nonlinearity within electroelastic micropower generators. *Applied Physics Letters* 97: 254101.

Stanton SC, McGehee CC and Mann BP (2009) Reversible hysteresis for broadband magnetopiezoelastic energy harvesting. *Applied Physics Letters* 96: 174103.

Stanton SC, McGehee CC and Mann BP (2010b) Nonlinear dynamics for broadband energy harvesting: Investigation of a bistable inertial generator. *Physica D* 239: 640–653.

Timoshenko SP, Young DH and Weaver W (1974) *Vibration Problems in Engineering*. New York: John Wiley & Sons.

Wang L and Yuan FG (2008) Vibration energy harvesting by magnetostrictive material. *Smart Materials and Structures* 17: 045009.

Williams RB, Park G, Inman DJ and Wilkie WK (2002) An overview of composite actuators with piezoceramic fibers. *Proceedings of the 20th International Modal Analysis Conference* 4753: 421–427.